

Experimental g factors and $B(E2)$ values of 2_1^+ , 4_1^+ , 2_2^+ , and 3_1^- states in ^{64}Zn and ^{68}Zn compared to shell model predictions

J. Leske, K.-H. Speidel, S. Schielke, O. Kenn, and D. Hohn

Helmholtz-Institut für Strahlen- und Kernphysik, Universität Bonn, Nussallee 14-16, D-53115, Germany

J. Gerber

Institut de Recherches Subatomiques, F-67037 Strasbourg, France

P. Maier-Komor

Physik-Department, Technische Universität München, James-Frank-Str., D-85748 Garching, Germany

(Received 6 October 2004; published 8 March 2005)

The g factors of the short-lived 2_1^+ , 4_1^+ , and 3_1^- states in ^{64}Zn and the 2_1^+ , 4_1^+ , 2_2^+ , and 3_1^- states in ^{68}Zn have been measured using the combined technique of projectile Coulomb excitation in inverse kinematics and transient magnetic fields. In addition, $B(E2)$'s have been deduced from remeasured lifetimes of several excited states employing the Doppler-shift-attenuation method. Whereas the present data for the 2_1^+ states agree very well with our previous results, the g factors of the other states have been determined for the first time. All experimental data were compared with results from large-scale shell model calculations based on proton and neutron configurations in the fp and fp g model spaces with ^{40}Ca and ^{56}Ni as inert cores, respectively.

DOI: 10.1103/PhysRevC.71.034303

PACS number(s): 21.10.Ky, 25.70.De, 27.50.+e

I. INTRODUCTION

In the following contribution we report on a series of new measurements to improve our understanding of the nuclear structure of even- A Zn nuclei, by extending the existing information on the two stable isotopes, ^{64}Zn and ^{68}Zn . These two nuclei are characterized by two protons and six or ten neutrons in the valence space of the $N = Z = 28$ closed ^{56}Ni core, respectively. Our earlier investigations, based on g factor and lifetime measurements, focused on systematics of the first 2^+ states of all stable even-even Zn isotopes [1]. These experiments were supplemented by similar investigations on the radioactive ^{62}Zn nucleus, which was produced in an α -transfer reaction from a ^{12}C target to an energetic ^{58}Ni beam [1]. With this nuclear reaction, a novel technique for determining g factors, lifetimes, and feeding patterns in radioactive nuclei was established under the same favorable conditions as in projectile Coulomb excitation experiments employing inverse kinematics. This method has so far been successfully applied to the spectroscopy of radioactive ^{44}Ti ($T_{1/2} = 60$ yr) [2] and ^{68}Ge ($T_{1/2} = 270$ d) [3] using ordinary stable beams of ^{40}Ca and ^{64}Zn , respectively. In both cases, the 2_1^+ states were preferentially populated, which allowed the deduction of the g factors from the measured precessions without requiring any significant correction for contributions from high-lying states. This selective excitation is a clear signature of the particle transfer mechanism, contrary to the excitation pattern associated with fusion reactions, which is characterized by cascade transitions from high-excitation and high-angular-momentum states along the yrast line. In such a situation, the feeding from high-spin states via cascade transitions is the dominant process. The g factors and lifetimes of these precursor states constitute the principal contribution to the precession of a low-lying nuclear state, dominating over the contribution from the state itself.

For the interpretation of the nuclear structure of zinc isotopes, large-scale shell model (LSSM) calculations were carried out. These exhibit rather subtle dependencies of g factors and $B(E2)$ values on spin and neutron number that were supported by some experimental data [1]. In these calculations two different model spaces have been considered: (i) a closed ^{40}Ca core plus valence protons and neutrons in the $f_{7/2}$, $p_{3/2}$, $f_{5/2}$, and $p_{1/2}$ orbitals (for computational reasons the $g_{9/2}$ orbital had to be excluded); (ii) a closed ^{56}Ni core plus the remaining fp shell orbitals, but with the explicit inclusion of the $g_{9/2}$ orbital. This intruder orbital should play a major role in the heavier Zn isotopes and for higher angular momentum states owing to its high- j orbital nature. It is notable that for heavy, odd Zn isotopes, isomeric $9/2^+$ states appear at relatively low excitation energies, suggesting the increasing influence of this orbital on the nuclear wave functions of low-lying states of the even- A Zn nuclei [4].

Whether excitations of the ^{56}Ni core are essential for the structure of the Zn nuclei as anticipated by the experimental data for the Ni isotopes [5] was a key question and a major motivation for the former and present measurements. This particular aspect should manifest itself through better agreement of the experimental data with results of the ^{40}Ca core calculations. Indeed the previous $g(2_1^+)$ values and $B(E2)$'s of the ($2_1^+ \rightarrow 0_1^+$) transitions of the lighter Zn isotopes were in fair agreement with those calculations [1]. Marked deviations revealed by the calculations for the heavier isotopes were mainly attributed to the exclusion of the $g_{9/2}$ orbital in the ^{40}Ca core. In these cases the results of the calculations with a ^{56}Ni core were indeed in better agreement with the data. More specifically, the calculated $B(E2)$'s of the ($4_1^+ \rightarrow 2_1^+$) transitions exhibit large variations depending on the inert core used for the calculations.

In view of these results and the discrepancies associated with the shell model predictions, new measurements have been performed to clarify this situation. The g factors of higher excited states as well as the corresponding $E2$ transition probabilities should provide sufficient information, with the magnetic moment as a sensitive probe for single-particle and the $B(E2)$'s for collective degrees of freedom, respectively. For these investigations two isotopes were chosen, ^{64}Zn and ^{68}Zn . The first is representative for the structure of the lighter Zn isotopes (where the two core shell model calculations yield almost identical results for the $B(E2; 4_1^+ \rightarrow 2_1^+)$'s [1]), whereas the experimentally determined lifetime for the second should enable a clear distinction between the two $B(E2)$ predictions. It is notable that the ^{40}Ca core calculations predict the $g(4_1^+)$ to be substantially larger than the $g(2_1^+)$, in contrast to comparable values obtained with an assumed ^{56}Ni core. This different behavior is due to the effect that the neutron of the included $g_{9/2}$ orbital has a negative g factor because its Schmidt value $g(vg_{9/2}) = -0.425$, using the bare values of $g_S = -3.826$ and $g_I = 0$.

II. EXPERIMENTAL DETAILS

The present measurements were carried out in the same way as those reported in [1]. The only difference was the elevated beam energy required to excite the high-lying states of interest. Isotopically pure beams of ^{64}Zn and ^{68}Zn were provided in their natural abundances as ZnO^- by the ion source of the Munich tandem accelerator and accelerated to an energy of 180 MeV (in contrast to the previous energy of only 160 MeV) with intensities of about 25 e nA on the target. The beam ions were Coulomb excited up to level energies of ~ 3 MeV by scattering from a natural carbon layer of a multilayered target.

Four slightly different targets (a–d) were used in the measurements of both isotopes. Their detailed compositions are summarized in Table I. In comparison to earlier targets (see, e.g., [1]), the new targets (b–d) incorporated very thin layers of natural titanium sandwiched between carbon and gadolinium as well as between tantalum and the copper backing. This new preparation technique significantly improved the adherence of the thick carbon layers to the surface of the Gd layers [6]. Sequential evaporations ensured that all target layers were in excellent contact with adjacent layers. For all targets the same good magnetization of the Gd layers was found [7]; external fields of 0.06 Tesla were sufficient to achieve saturation magnetizations at liquid nitrogen temperature, close to the

TABLE I. Composition of the multilayered targets used in the measurements.

Target	Layer thickness (mg/cm ²)					
	C	Ti	Gd	Ta	Ti	Cu
a	0.355	—	4.40	1.1	—	3.40
b	0.500	0.005	3.26	1.8	0.005	4.25
c	0.442	0.005	3.34	1.4	0.005	4.49
d	0.460	0.005	3.61	1.6	0.005	4.20

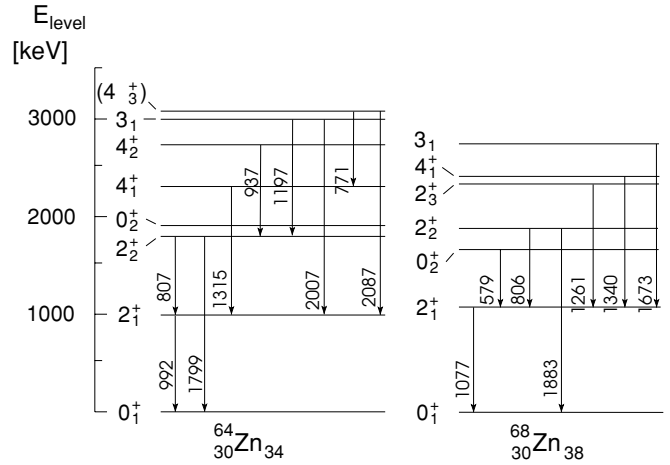


FIG. 1. Low-lying states and γ transitions of ^{64}Zn and ^{68}Zn relevant to the present measurements.

theoretical value [8]. The Coulomb excited Zn nuclei moved at high velocities ($v_{\text{ion}} \simeq 6.5v_0$, $v_0 = e^2/\hbar$) in the direction of the primary beam through the Gd layer in which they experienced the transient fields (TF) for spin precessions and were ultimately stopped in the copper backing, which served as a hyperfine interaction-free environment.

The deexcitation γ rays emitted from the excited states of the two isotopes (Fig. 1) were measured in coincidence with the forward scattered carbon ions detected in a 100 μm Si detector at 0° . A Ta foil between the target and the detector served as a beam stopper, which, however, was transparent to the carbon recoils. The Si detector was operated at a low bias of $\simeq 5$ V (instead of the nominal 40 V), to separate protons and α particles (originated in fusion and transfer reactions) from the carbon ions via their different stopping power in the reduced depletion layer of the particle detector.

Four 12.7 cm \times 12.7 cm NaI(Tl) scintillators and an intrinsic Ge detector of 40% relative efficiency were used for γ detection. Coincident γ -ray spectra from the Ge detector are displayed in Fig. 2. The particle gates were set only on the broad energy distribution of the carbon ions, giving rise to γ lines associated exclusively with the excited Zn nuclei. Hence, very clean spectra were obtained, in which the Doppler-broadened line shapes reflect the nuclear lifetimes (see the following discussion). The corresponding spectra of the scintillators are shown in Fig. 3. When comparing them to the Ge spectra, it becomes evident that the prominent lines are those of the $(2_1^+ \rightarrow 0_1^+)$, $(4_1^+ \rightarrow 2_1^+)$, and $(3_1^- \rightarrow 2_1^+)$ transitions for ^{64}Zn and in addition the $(2_2^+ \rightarrow 0_1^+)$ transition for ^{68}Zn . All these lines are resolved in the γ spectra, allowing a rigorous determination of their intensities, as required for the angular correlations as well as for the precessions of the nuclear states in question.

However, for ^{68}Zn the $(4_1^+ \rightarrow 2_1^+)$ γ line of 1340 keV was not completely resolved from the neighboring $(2_3^+ \rightarrow 2_1^+)$ 1261 keV line, in particular in the spectra of the forward detectors owing to the large Doppler shift of the latter. In spite of this difficulty, the intensity of the $(4_1^+ \rightarrow 2_1^+)$ transition was determined by setting a narrow window on the peak

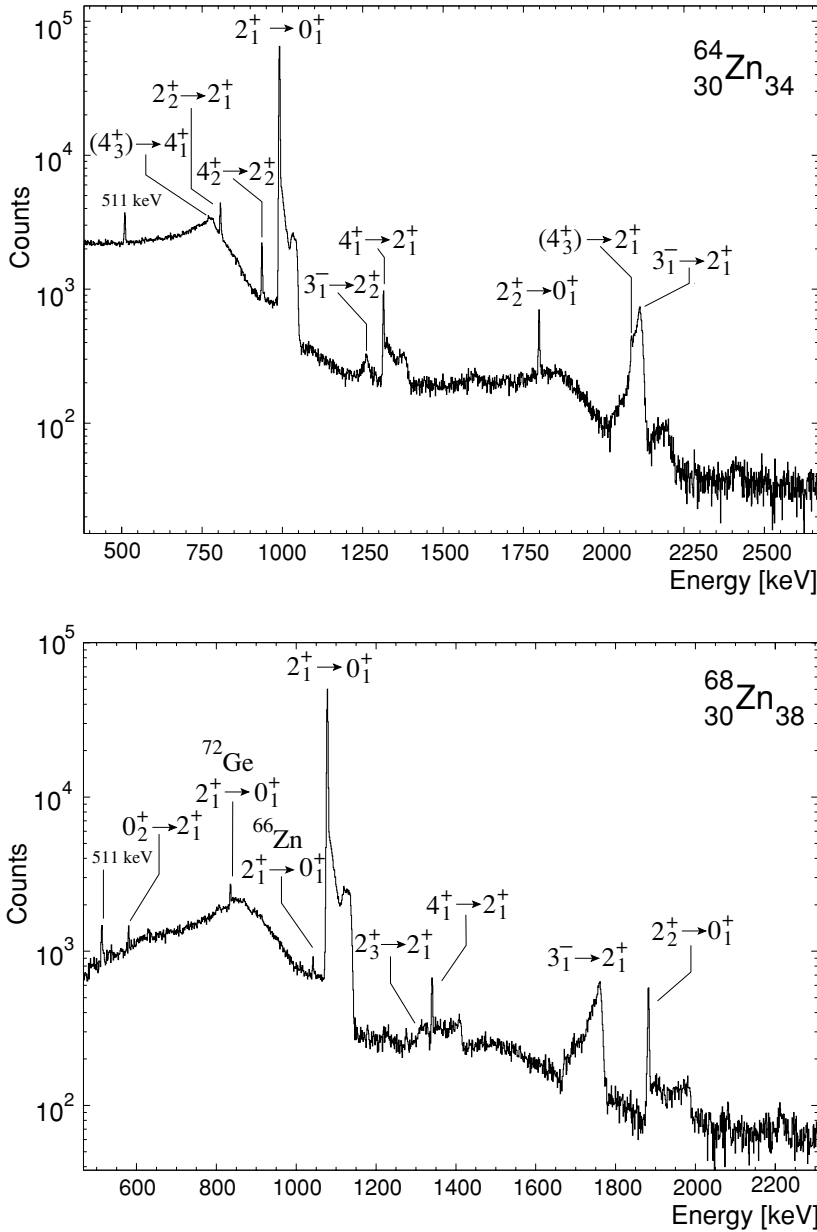


FIG. 2. γ -coincidence spectra for ^{64}Zn and ^{68}Zn observed with a Ge detector placed at $\Theta_\gamma = 0^\circ$ relative to the beam direction. Most of the γ lines are identified according to the relevant level schemes (Fig. 1). Doppler-broadened line shapes reflect the nuclear lifetimes.

and subtracting background resulting essentially from the Compton-scattered γ rays of the $(3_1^- \rightarrow 2_1^+)$ transition.

Detailed particle- γ -angular correlations $W(\Theta_\gamma)$ and anisotropies $W(\Theta_\gamma = 50^\circ)/W(\Theta_\gamma = 80^\circ)$ have been measured for all relevant transitions of each isotope. This was done to determine the logarithmic slopes, $|S| = [1/W(\Theta_\gamma^{rf})] \cdot [dW(\Theta_\gamma^{rf})/d\Theta_\gamma^{rf}]$ in the rest frame (rf) of the γ -emitting nuclei at laboratory angles $\Theta_\gamma^{\text{lab}} = \pm 65^\circ$ and $\pm 115^\circ$, at which the sensitivity to the spin precessions was optimal for all transitions in question. The slopes, measured with the γ scintillators placed in pairs symmetric to the beam direction, are summarized in Table II. Precession angles, Φ^{exp} , were derived from double ratios R of coincident counting rates for external fields perpendicular to the γ -detection plane, alternately in the “up” and “down” directions. The precession angles can be expressed as

$$\Phi^{\text{exp}} = \frac{1}{S} \cdot \frac{\sqrt{R} - 1}{\sqrt{R} + 1} = g \frac{\mu_N}{\hbar} \int_{t_{\text{in}}}^{t_{\text{out}}} B_{\text{TF}}(v_{\text{ion}}(t)) e^{-\frac{t}{\tau}} dt, \quad (1)$$

where g is the g factor of the excited state and B_{TF} the transient field acting on the nucleus during the time interval $(t_{\text{out}} - t_{\text{in}})$ spent by the ions in the Gd layer; the exponential accounts for nuclear decay during the transit time of the ions through the gadolinium layer.

The lifetimes of several excited states have been measured using the DSAM technique. The high ion velocities ensured high sensitivity for lifetimes in the ps and sub- ps ranges. The Doppler-broadened shapes of the γ -ray lines were fitted for the reaction kinematics by applying stopping powers [9] to Monte Carlo simulations and including the second-order Doppler effect as well as the finite size and the energy resolution of the Ge detector. Feeding from higher states was also included,

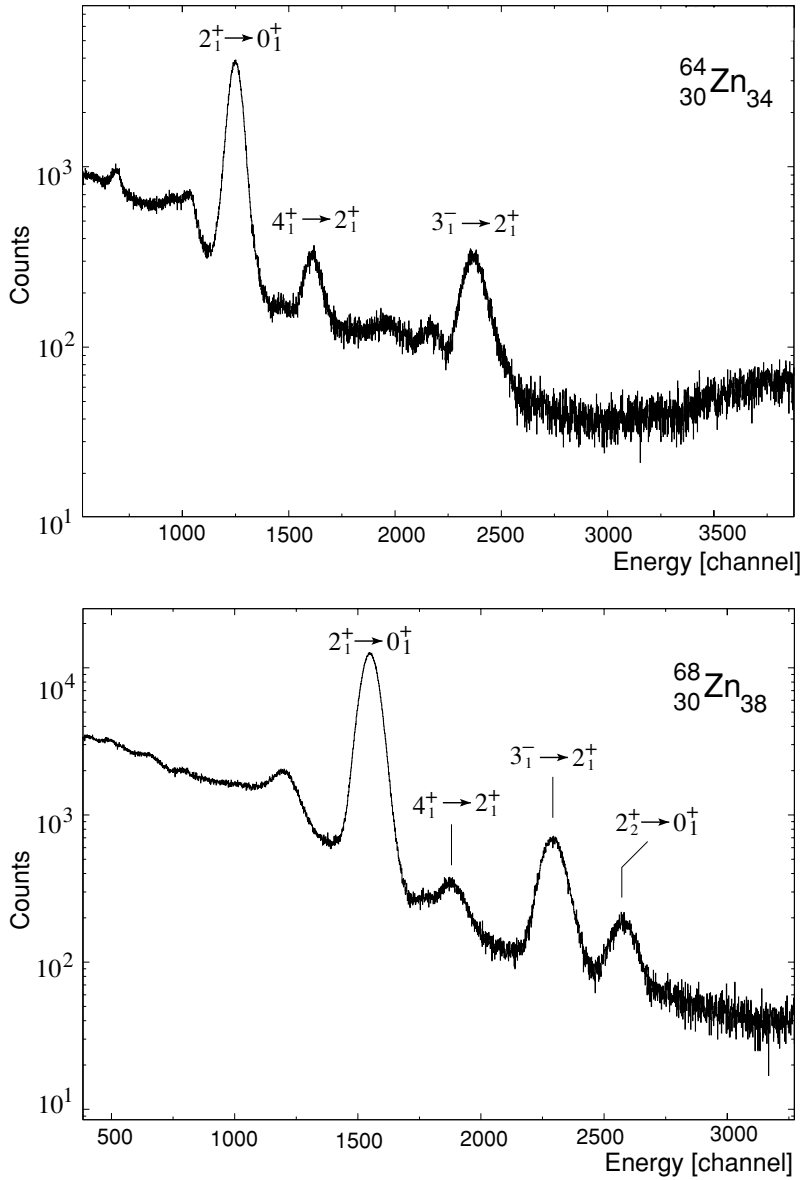


FIG. 3. γ -coincidence spectra for ^{64}Zn and ^{68}Zn observed with a large-volume NaI(Tl) scintillator placed at $\Theta_\gamma = 65^\circ$. The assigned transitions refer to the present investigations (see text).

which was specifically important for the lifetime of the 2_1^+ states in both isotopes, which exhibit feeding contributions to the stopped component of $\simeq 10\%$. The computer code LINESHAPE [10] was used in the analysis. The high-quality fits of typical line shapes are shown in Figs. 4 and 5. It is noted that characteristic structures in the shapes of the γ lines, resulting from the slowing down of the ions in the different target layers, were very well reproduced. One can easily distinguish three regions in the shape curve; these are associated with the three main target layers of carbon, gadolinium, and copper. The lifetimes deduced are summarized in Table III together with adopted values from the literature.

III. RESULTS AND DISCUSSION

The g factors were derived from the measured precession angles using the effective transient field B_{TF} on the basis of

the empirical linear parametrization (see, e.g., [1,11]):

$$B_{\text{TF}}(v_{\text{ion}}) = G_{\text{beam}} \cdot B_{\text{lin}} \tag{2}$$

with

$$B_{\text{lin}} = a(\text{Gd}) \cdot Z_{\text{ion}} \cdot (v_{\text{ion}}/v_0), \tag{3}$$

where the strength parameter $a(\text{Gd}) = 17(1)$ Tesla [11] and $G_{\text{beam}} = 0.61(6)$ is the attenuation factor accounting for the demagnetization of the Gd layer induced by the Zn beams. Its value was derived by interpolation of numerous data for the current experimental conditions in terms of the energy loss of the beam ions and the ion velocity of the excited nuclei in the Gd layer [11].

The experimental precession angles are summarized in Table II. For both isotopes several runs were needed to obtain sufficient accuracy for the states beyond the 2_1^+ state. The causes of the limited accuracy are the reduced excitation cross sections (compared to those of the 2_1^+ states) and also the much

TABLE II. Summary of the measured logarithmic slopes of the angular correlations at $|\Theta_{\gamma}^{rf}|$ and the precession angles Φ^{exp} . The Φ^{lin}/g values were calculated using Eqs. (1)–(3). Only in run I was the beam energy 175 MeV, whereas in all other runs the energy was 180 MeV. 9 cm \times 9 cm BaF₂ detectors were used in the runs marked with asterisks, whereas in all other runs NaI(Tl) scintillators were used (see text).

Nucleus	I^{π}	$E_x(I^{\pi})$ (MeV)	Run	Target	$ S(\Theta_{\gamma}^{rf}) $ ([mrad] ⁻¹)	Φ^{exp} (mrad)	Φ^{lin}/g (mrad)
⁶⁴ Zn	2_1^+	0.992	I ^(*)	a	2.052(98)	15.4(8)	34.8(3.4)
			II	b	1.683(20)	12.1(3)	26.1(2.6)
			II ^(*)		1.946(31)	12.4(3)	
			III	c	0.808(16)	10.7(8)	25.3(2.7)
	4_1^+	2.307	I ^(*)	a	0.7(2)	10(15)	30.2(3.0)
			II	b	0.563(30)	13(7)	23.2(2.3)
			II ^(*)		0.651(37)	19(9)	
			III	c	0.751(96)	11(5)	22.6(2.4)
	3_1^-	2.998	I ^(*)	a	0.311(10)	13(9)	13.9(1.4)
			II	b	0.257(37)	2(5)	11.0(1.1)
			II ^(*)		0.268(63)	2(7)	
			III	c	0.265(47)	13(8)	12.1(1.3)
⁶⁸ Zn	2_1^+	1.077	I	d	1.571(24)	14.6(1.1)	28.6(2.8)
			II		1.486(20)	14.4(3)	
	4_1^+	2.417	II	d	0.75(10)	-11(5)	25.7(2.5)
	3_1^-	2.751	II	d	0.240(42)	7(6)	17.8(1.8)
	2_2^+	1.883	I	d	1.19(32)	9(9)	26.9(2.6)
			II		1.06(13)	15(4)	

weaker anisotropies of the corresponding angular correlations, as evident from the magnitude of their slope values (Table II). The precessions Φ^{lin}/g , which are also listed in Table II, have been calculated using Eqs. (1)–(3) with the lifetimes determined in the present measurements (Table III). The g factors deduced are summarized in Table III.

Evidently, for both isotopes, several newly determined lifetime values differ from those quoted in the literature. Good

agreement was achieved for the 2_1^+ , 2_3^+ , and 4_3^+ states. In particular, for the first 2^+ states, our previous accurate values have been well confirmed [1]. It is further notable that the lifetimes of Table III are averages over two or three runs, which were required to enhance the precision of the g factors in question. The overall consistency of the g factor results from the individual runs is illustrated in Fig. 6. $B(E2)$ values have been deduced in Weisskopf units from the measured lifetimes

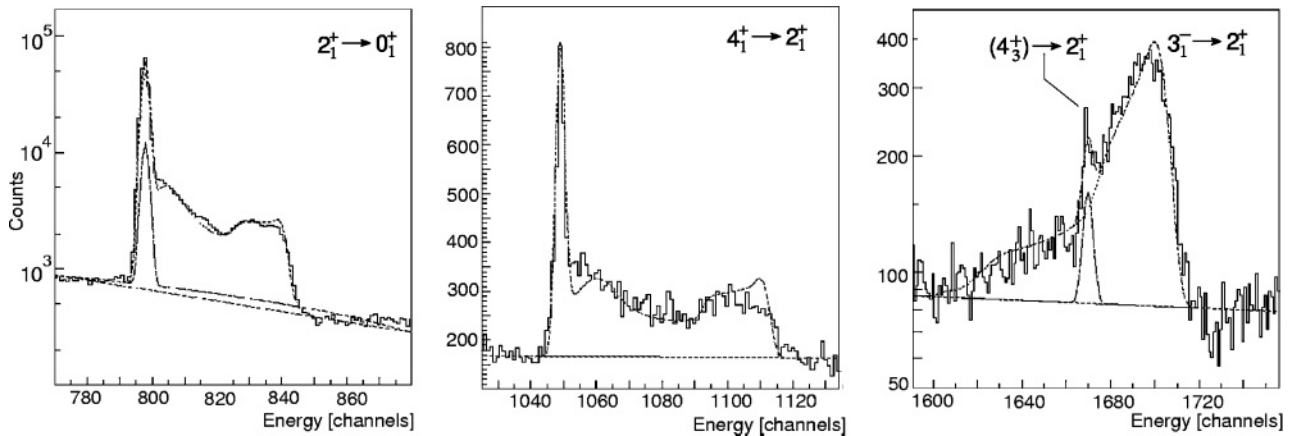


FIG. 4. DSAM fits to the Doppler-broadened shapes of γ lines in ⁶⁴Zn. The contribution of feeding from higher states to the stopped component of the ($2_1^+ \rightarrow 0_1^+$) γ line is also displayed.

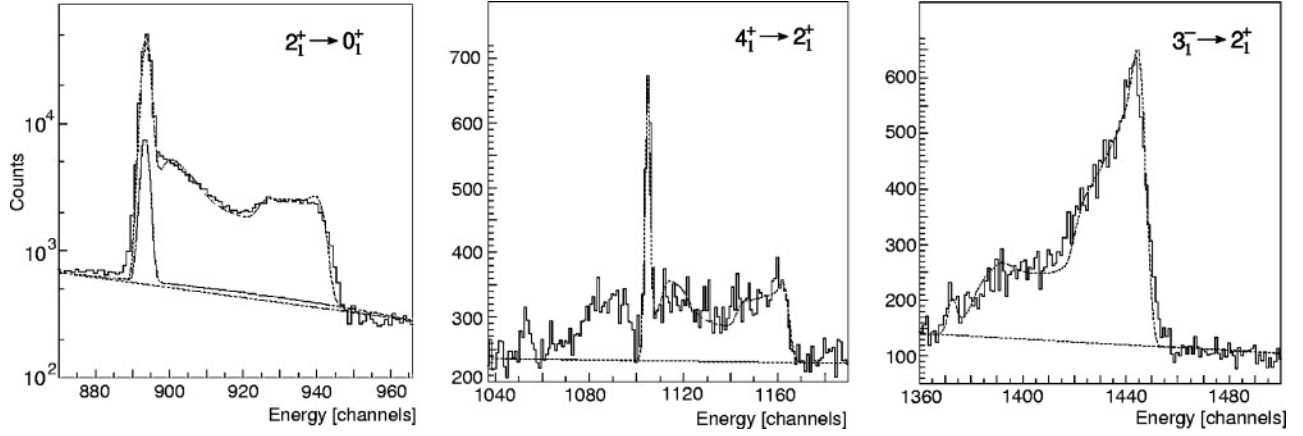


FIG. 5. DSAM fits to the Doppler-broadened shapes of γ lines in ^{68}Zn . The contribution of feeding from higher states to the stopped component of the ($2_1^+ \rightarrow 0_1^+$) γ line is also displayed.

and were compared with shell model predictions, as shown in Table IV.

Both the new g factor and $B(E2)$ data of the present work were compared with results of former large-scale shell model calculations assuming two different configuration spaces: model space I (LSSM I) refers to a closed ^{40}Ca core, and model space II (LSSM II) is based on a closed ^{56}Ni core including the intruder $g_{9/2}$ orbital. All other details of these calculations are discussed in [1]. It is noted that results of the same calculations were already used to explain previous data, which, however, referred exclusively to the 2_1^+ states of several Zn isotopes [1,14]. The different predictions of the two calculations for the g factors and the $B(E2)$'s are compared to each other and with experimental data in Table IV. The results for the 2_1^+ and 4_1^+ states are also displayed, along with our previous data for the other Zn isotopes, in Fig. 7. In the g factor plots, the Z/A values of the hydrodynamical model are also shown.

TABLE III. Comparison of the measured lifetimes and g factors with data from literature. The g factors are the weighted mean values of results from different runs (see Fig. 6).

Nucleus	I^π	τ [ps]		$g(I^\pi)$	
		Refs.	Present	Refs.	Present
^{64}Zn	2_1^+	2.70(8) ^a	2.85(9)	+0.445(46) ^a	+0.447(29)
	4_1^+	0.48(10) ^b	1.12(4)	—	+0.53(16)
	3_1^-	0.127(22) ^b	0.220(6)	—	+0.5(3)
	(4_3^+)	0.71(17) ^b	0.79(9)	—	—
^{68}Zn	2_1^+	2.32(7) ^a	2.32(5)	+0.436(47) ^a	+0.505(38)
	4_1^+	—	1.10(8)	—	-0.4(2)
	3_1^-	0.63(14) ^c	0.38(2)	—	+0.4(3)
	2_2^+	2.3(4) ^c	1.4(1)	—	+0.53(15)
	2_3^+	0.35(⁺¹⁶ ₋₉) ^c	0.45(4)	—	—

^a[1].

^b[12].

^c[13].

Whereas the $g(2_1^+)$ values of ^{64}Zn and ^{68}Zn are rather well described by both LSSM I and II, of which LSSM I is closer to the experimental data, the $g(4_1^+)$ value of ^{64}Zn is not precise enough to distinguish between the two calculations, despite the rather large difference in the calculated values: $g(\text{LSSM I}) = +0.73$ versus $g(\text{LSSM II}) = +0.362$ (see Table IV and [1]). Nevertheless, more preference is given to the LSSM II result, as, for high-angular-momentum states, the high- j orbitals should play a more important and therefore indispensable role (bearing in mind that in LSSM II the $g_{9/2}$ orbital has been explicitly included). However, the g factor of the 4_1^+ state also agrees with the collective value, $g = Z/A = 0.46$, supporting the vibrational picture of ^{64}Zn . This feature is further supported by the result that $g(2_1^+) = +0.447(29)$ agrees within errors with $g(4_1^+) = 0.53(16)$.

For ^{68}Zn the precession of the 4_1^+ state yielded a very surprising result for the g factor: $g(4_1^+) = -0.4(2)$ (see Tables III and IV), as it strongly contradicts the present shell model calculations LSSM I and II, both of which predict positive values (see Fig. 7). At the present time, this result must be considered with caution because of interferences of the ($4_1^+ \rightarrow 2_1^+$) γ line with adjacent γ lines in the scintillator spectra (see Figs. 2 and 3). However, for the backward detectors, where the separation of the ($4_1^+ \rightarrow 2_1^+$) γ line from the main disturbing 1261 keV line is significantly better owing to the large Doppler shift, the spin precession also yields a

TABLE IV. Comparison of present experimental g factors and $B(E2)$ values with results from large-scale shell model calculations LSSM I and II (see text).

Nucleus (I^π)	$B(E2)$ (W.u.)			$g(I^\pi)$		
	Expt.	LSSM I	LSSM II	Expt.	LSSM I	LSSM II
$^{64}\text{Zn}(2_1^+)$	19.5(6)	15.4	11.3	+0.447(29)	+0.48	+0.448
	(4_1^+)	12.2(4)	15.3	14.3	+0.53(16)	+0.73
$^{68}\text{Zn}(2_1^+)$	14.7(3)	9.0	9.7	+0.505(38)	+0.58	+0.733
	(4_1^+)	10.4(8)	3.3	10.9	-0.4(2)	+1.08

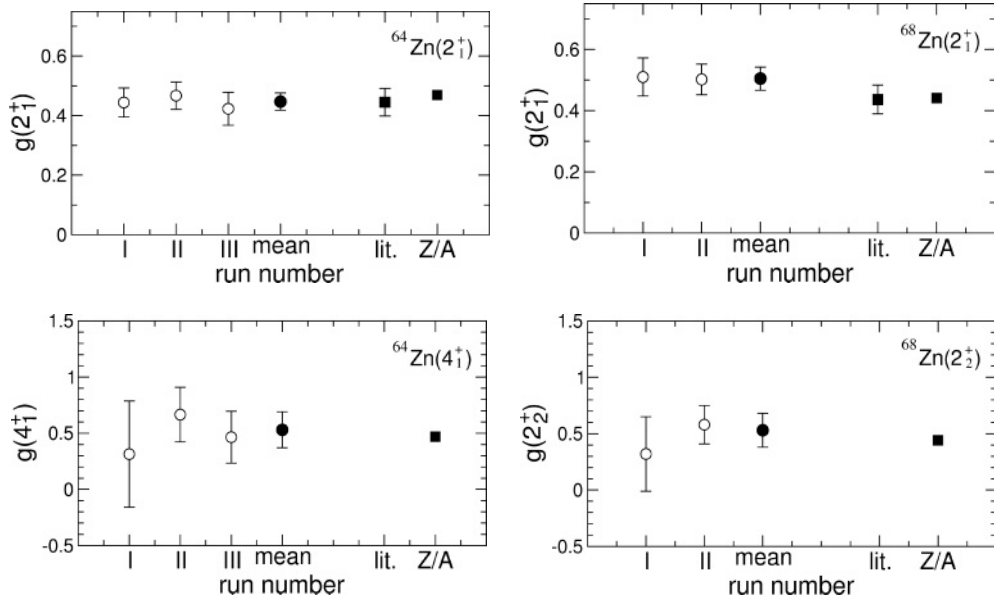


FIG. 6. Measured g factors for 2_1^+ and 4_1^+ in ^{64}Zn and 2_1^+ and 2_2^+ in ^{68}Zn vs run number, displayed along with weighted mean values and previous results [1]. The Z/A predictions of the collective model are also shown.

negative g value. Hence, the negative sign of the present g factor, if true, strongly suggests a dominating $g_{9/2}$ neutron component in the nuclear wave function, with its Schmidt value of $g(\nu g_{9/2}) = -0.425$ (see the following). This interpre-

tation was already suggested in the early work by Bruandet *et al.* [15], who stressed the point that the positive-parity high spin states ($I = 4^+, 6^+, 8^+$) in this nucleus are associated with neutron configurations $[(1f_{5/2})_0^+(1g_{9/2})^2]^I$. This very

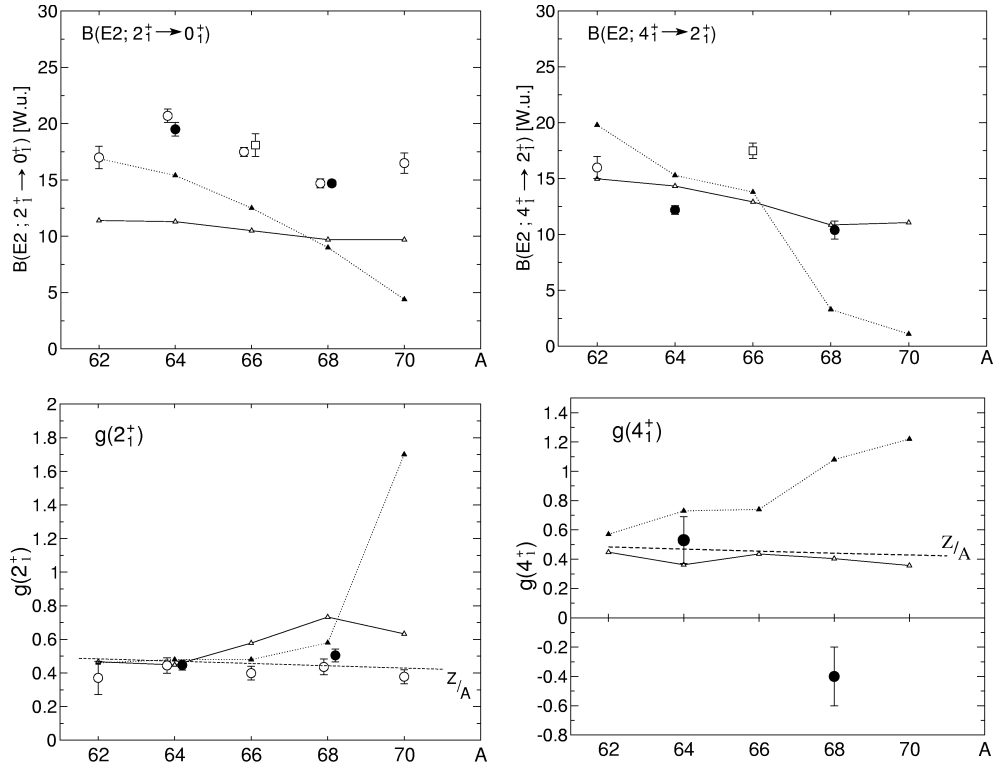


FIG. 7. Experimental g factors of 2_1^+ and 4_1^+ states and $B(E2)$ values of corresponding transitions in Weisskopf units compared with results from shell model calculations and Z/A predictions as a function of mass number in Zn nuclei. Closed (open) circles refer to present (previous) measurements; open squares represent recent data of Ref. [14]. The small triangles connected by dotted and solid lines refer to calculations with a ^{40}Ca core (LSSM I) and a ^{56}Ni core (LSSM II), respectively (see text).

interesting feature certainly justifies more experimental effort in performing measurements under improved conditions, for example, by using Ge detectors instead of scintillators, to avoid interferences of the γ lines by virtue of their superior energy resolution. Note that in a preliminary analysis of a newly performed measurement using Ge detectors, the negative sign of the g factor has been confirmed. Details of this investigation and the final result of the g factor will be presented in a forthcoming publication [16].

In contrast, the newly measured g factor of the 2_2^+ state at 1.883 MeV, $g(2_2^+) = +0.53(15)$, fits perfectly into a vibrational picture of ^{68}Zn with its prediction of $g(I) = Z/A = +0.44$. This collective behavior is also supported by the good agreement of $g(2_2^+)$ with the more precise result for the 2_1^+ state, $g(2_1^+) = +0.505(38)$.

Hence, on the basis of the measured g factors [with the exception of the debatable $^{68}\text{Zn}(4_1^+)$ value] the collective model seems to be very capable of explaining the nuclear structure of the low-lying states in both ^{64}Zn and ^{68}Zn . The amount of collectivity is, however, well accounted by shell model calculations based on the extended configuration space of fpg -shell orbitals and a closed ^{56}Ni core. This collective scenario is supplemented by the g factors of the 3_1^- states in both ^{64}Zn and ^{68}Zn , which were determined for the first time. The values obtained for ^{64}Zn , $g(3_1^-) = +0.5(3)$ and for ^{68}Zn , $g(3_1^-) = +0.4(3)$ are both consistent with the predictions for octupole vibrations, $g = Z/A = 0.47$ and 0.44 , respectively. It is noted that the low accuracy of the data is primarily a consequence of the weak anisotropy of the angular correlations of the corresponding ($3_1^- \rightarrow 2_1^+$) γ transitions.

A more sensitive quantity for determining the collective behavior is the $B(E2)$ value. For the ($2_1^+ \rightarrow 0_1^+$) transitions of the even- A Zn isotopes, the $E2$ strengths are between 15 and 20 W.u. (Fig. 7 and Table IV). Both shell model calculations, using effective charges for neutrons and protons of $0.5 e$ and $1.5 e$, respectively, generally underestimate the experimental values but reproduce very well the decreasing trend observed from ^{64}Zn to ^{68}Zn (see also [5]). Specifically, the LSSM I results with its ^{40}Ca core show better agreement with the observed variations. The experimental data clearly exhibit

a minimum at $A = 68$, which might reflect a neutron $f_{5/2}$ subshell closure. This feature is further supported by the result of a recent measurement on the $^{72}\text{Zn}(2_1^+)$ state yielding the value $B(E2) = 20(2)$ W.u. [17], which is significantly larger than that of ^{68}Zn and ^{70}Zn .

The $B(E2)$'s of the ($4_1^+ \rightarrow 2_1^+$) transitions in $^{64,68}\text{Zn}$, which were determined for the first time, are well explained by the LSSM II calculations with a closed ^{56}Ni core and the inclusion of the $g_{9/2}$ intruder orbital. Evidently, the experimental strength for ^{68}Zn is larger than the result from the ^{40}Ca core calculations (LSSM I) (see Fig. 7). This behavior is also supported by a recent $B(E2)$ measurement for ^{66}Zn [14]. In fact, the experimental result in this case is not only larger than the shell model prediction but also significantly exceeds the experimental values for neighboring ^{64}Zn and ^{68}Zn (Fig. 7).

IV. SUMMARY AND CONCLUSION

For the two Zn isotopes, ^{64}Zn and ^{68}Zn , g factors and lifetimes have been measured for several excited states above the 2_1^+ states. The lifetimes and the deduced $B(E2)$'s of the 4_1^+ states were determined for the first time. The new g factor values for the 4_1^+ and 3_1^- states in ^{64}Zn and the 2_2^+ and 3_1^- states in ^{68}Zn are consistent with predictions of the vibrational model. A very surprising result was obtained for the $^{68}\text{Zn}(4_1^+)$ state: Its negative g factor suggests a dominant $g_{9/2}$ neutron component in the nuclear wave function. The amount of collectivity is generally well accounted for by large-scale fpg shell model calculations based on a closed ^{56}Ni core and including the $g_{9/2}$ intruder orbital. The experimental $B(E2)$ for the ($2_1^+ \rightarrow 0_1^+$) transition in ^{68}Zn indicates neutron $f_{5/2}$ subshell closure, that applies to lower spin states but no longer to the 4_1^+ state.

ACKNOWLEDGMENTS

The authors are grateful to the operators of the Munich tandem accelerator for their extraordinary cooperation in providing optimum beam conditions during the runs. Support by the BMBF and the Deutsche Forschungsgemeinschaft is acknowledged.

-
- [1] O. Kenn, K.-H. Speidel, R. Ernst, S. Schielke, S. Wagner, J. Gerber, P. Maier-Komor, and F. Nowacki, Phys. Rev. C **65**, 034308 (2002).
- [2] S. Schielke, K.-H. Speidel, O. Kenn, J. Leske, N. Gemein, M. Offer, Y. Y. Sharon, L. Zamick, J. Gerber, and P. Maier-Komor, Phys. Lett. **B567**, 153 (2003).
- [3] J. Leske, K.-H. Speidel, S. Schielke, O. Kenn, J. Gerber, P. Maier-Komor, S. J. Q. Robinson, Y. Y. Sharon, and L. Zamick, submitted to Phys. Rev. C.
- [4] P. Herzog, U. Dämmrich, K. Freitag, C.-D. Herrmann, and K. Schlösser, Z. Phys. A **332**, 247 (1989).
- [5] O. Kenn, K.-H. Speidel, R. Ernst, J. Gerber, N. Benczer-Koller, G. Kumbartzki, P. Maier-Komor, and F. Nowacki, Phys. Rev. C **63**, 021302(R) (2000).
- [6] P. Maier-Komor, R. Krücken, K.-H. Speidel, and O. Kenn, Nucl. Instrum. Methods Phys. Res. A **521**, 17 (2004).
- [7] P. Maier-Komor, K.-H. Speidel, and A. Stolarz, Nucl. Instrum. Methods Phys. Res. A **334**, 191 (1993).
- [8] C. Kittel, *Introduction to Solid State Physics* (Wiley, New York, 1976).
- [9] F. J. Ziegler, J. Biersack, and U. Littmark, *The Stopping and Range of Ions in Solids* (Pergamon, Oxford, 1985), Vol. 1.
- [10] J. C. Wells and N. R. Johnson, program LINESHAPE, ORNL, 1994.
- [11] K.-H. Speidel, O. Kenn, and F. Nowacki, Prog. Part. Nucl. Phys. **49**, 91 (2002).
- [12] B. Singh, Nucl. Data Sheets **78**, 395 (1996).

- [13] T. W. Burrows, Nucl. Data Sheets **97**, 1 (2002).
- [14] M. Koizumi, A. Seki, Y. Toh, M. Oshima, A. Osa, A. Kimura, Y. Hatsukawa, T. Shizuma, T. Hayakawa, M. Matsuda, J. Katakura, T. Czosnyka, M. Sugawara, T. Morikawa, and H. Kusakari, Eur. Phys. J. A **18**, 87 (2003).
- [15] J. F. Bruandet, B. Berthet, C. Morand, A. Giorni, J. P. Longequeue, and T. U. Chan, Phys. Rev. C **14**, 103 (1976).
- [16] J. Leske, K.-H. Speidel, S. Schielke, J. Gerber, and P. Maier-Komor (to be published).
- [17] S. Leenhardt *et al.*, Eur. Phys. J. A **14**, 1 (2002).